AUT Journal of Mechanical Engineering

AUT J. Mech. Eng., 4(3) (2020) 315-330
DOI: 10.22060/ajme.2019.16920.5841

Investigation of an Adsorptive Indigo Carmine Dye Removal via Packed Bed Column: Experiments and Computational Fluid Dynamics Simulation

Z. Hosseini Dastgerdi, S. S. Meshkat*, H. Jalili

Faculty of Chemical Engineering, Urmia University of Technology, Urmia, Iran

ABSTRACT: In this study, the experiments and computational fluid dynamics simulations were carried out to determine the removal efficiency of the indigo carmine dye from wastewater via graphene nanoadsorbent. The adsorption process was done in a packed bed column. The synthesized nanoporous graphene via chemical vapor deposition method was characterized by Brunauer-Emmett-Teller, scanning microscopy and X-ray Diffraction techniques. Batch adsorption experiments were conducted, and Langmuir isotherm was best fitted to the experimental data. A parallel series of fixed bed column adsorption and desorption tests was done. The breakthrough curves were investigated by varying indigo carmine dye solution flow rate (1–10 ml/min), indigo carmine dye solution concentration (10–100 ppm) and adsorbent bed depth (10–28 cm). The reusability of adsorbent was studied. The computational fluid dynamics simulation was used for the three-dimensionally simulation of flow patterns and dye concentration changes in the packed bed column throughout the adsorption. High bed depth, low flow rate and high initial dye concentration were recommended to be the potential parameters for the high adsorption capacity. The conformity of the experimental test with the computational fluid dynamic calculations was a suitable methodology method to prove the reliability of the dye adsorption process. The removal efficiency of indigo carmine dye was achieved to be 67% as flow rate, bed depth, and concentration of 1 ml/min, 28 cm and 10 ppm, respectively.

Review History:
Received: 2019-08-15
Revised: 2019-11-10
Accepted: 2019-12-09
Available Online: 2019-12-26

Keywords:
Indigo carmine dye
Adsorption
Fixed bed column
Computational fluid dynamics
Graphene

1. INTRODUCTION

The effluent release of different industries, such as paper, textile, carpet, plastics, dying, leather, pharmaceutical, and food industries into streams causes threats to the environment and human communicates. As a result, these industries generate a considerable quantity of dye [1-3]. The reports indicate that over 100000 commercially available dyes exist and additionally above 7×10^5 ton are produced annually in all over the world [4,5]. Most of the dye compounds are resistant to biodegrading. The presence of a very small quantity of dyes in water (about 1 ppm) can be easily visible and is unattractive [5]. Indigo Carmine (IC) is deliberated as one of the highest toxic pigment. It is used as a pH effector in analytical chemistry as a dye for different industries [6].

The different methods are known for wastewater treatment. The main dye treatment methods include: chemical oxidation [7], coagulation [8], membrane separation process [9], exchange of ions [10], electrochemical [11] and aerobic and anaerobic microbial degradation [12], adsorption process [13]. One of the most favorable methods of dye removal is the adsorption process. The simplicity, ambient temperature and pressure, low cost process and high removal efficiency make the adsorption process one of the effective dye removal methods [14]. There are different adsorbents for the remediation of several impurities such as dyes from wastewater [15,16]. Carbon based materials are the most common adsorbent due to their high capacity in adsorption process and higher surface area for the adsorption and low-cost synthesis method [17]. Because of increasing demand in wastewater treatment industry, high reusable and eco-environment adsorbent with low cost is motivating researchers into the synthesis of carbon based adsorbents from alternative precursors, such as agricultural solid wastes and by- products [18]. There has been much effort in recent years to explore the use of agricultural filtrates and unavoidable by-products.

The equilibrium data and adsorbent capacity are calculated in batch experiments. The batch experiments are not capable of covering the continuous process. In continuous adsorption process, the contact time is sufficient enough to remove the organic pollutants such as IC dye. Because of the high solubility of dyes in water, the usual dye removal methods are inefficient. For wastewater treatment, the continuous fixed bed adsorption systems are generally used. In continuous systems, a single column is loaded with the utilization of synthesized adsorbent. The removal of indigo carmine dye from wastewater effluents in continuous fixed bed columns is reported [17,18]. Singh and Pant [19] evaluated the adsorptive removal of as ions in a fixed bed column utilization of activated alumina, iron oxide impregnated activated alumina. Results

*Corresponding author's email: s.meshkat@che.uut.ac.ir

proved that the adsorbent is suitable for the adsorption of As ions. Banejree et al. [20] researched the use of pistachio shell in a continuous system for the adsorption of IC dye. They evaluated the effect of IC dye initial concentration on the breakthrough curve. In this research, due to the large specific surface area, honey ball structure and aromatic cycles in configuration of the graphene. The graphene was synthesized and selected as an adsorbent in the continuous system [21]. The removal efficiency of the synthesized adsorbent is the highest in the comparison of literature review. Because of the high capacity of the adsorbent, the synthesized adsorbent got saturated in the long period of time in comparison with the previous synthesized adsorbents. Different functional groups such as carboxyl in chemical structure of graphene create this carbon based material an effective adsorbent [22]. To the best of our knowledge, the application of graphene as the adsorbent for the removal of indigo carmine dye in fixed bed columns has not been studied yet.

Therefore, we synthesized graphene and used it as the adsorbent to investigate the removal of indigo carmine dye from aqueous solutions in dynamic process. The effect of inlet dye concentration, bed depth and flow rate of the adsorbate solution which are known as the design process parameters were investigated with the utilization of a laboratory fixed bed column. The regeneration of the saturated adsorbent was studied by desorption experiments. The results of the regeneration process make the graphene more suitable for the IC dye removal. The simulation of the adsorptive IC dye removal in the fixed bed column was done by Computational Fluid Dynamic (CFD) technique. The effect of inlet concentration of dye solution, inlet flow rate, and column bed height was investigated using Comsol Multiphysics software 5.3a.

2. MATERIAL AND METHODS

2.1. Synthesis of graphene

Synthesis of the graphene nanostructure was performed through Chemical Vapor Deposition (CVD) method. In this protocol, carbon source which is provided by methane gas (99.9%) was introduced into an electrical furnace containing a quartz tube reactor. The nanostructured graphene with an average diameter of 50 nm and length of 120 mm was formed on the surface of metal oxide nano catalysts in the quartz tube reactor. In addition, a carrier gas such as hydrogen was entered to the reactor with the methane to hydrogen ratio of 4:1. The gas mixture was distributed through the reactor for 10 min, and the temperature of the furnace hot zone was 900-1100 ^{0}C. Then, the purification of the synthesized graphene was done. The synthesized graphene was stirred in HCl solution for about 16 h then it was rinsed with distilled water several times to achieve the neutral pH [23].

2.2. Characterization techniques

The morphology and structure of nanostructured graphene was determined by Scanning Electron Microscopy (SEM). The SEM images were collected by employing a Tescan Mira device. X-Ray Diffraction (XRD) patterns were accomplished using the standard powder diffraction procedure done with a Philips diffractometer (PW- 1730) (Lump 3ukα, λ = 1.54 Å). Elemental analysis (CHN) was performed by Costech device, ECS4010 model in which the sample was burned at 1100 ^{0}C. The Brunauere–Emmett–Teller (BET) method was used to determine the BET surface area. Calculating the surface area, pore volume, and pore size distribution were done by adsorption/desorption under the nitrogen atmosphere at 77 K utilization of ASAP-2010 porosimeter from the Micromeritics Corporation GA. The pH point of zero charge (pHpzc) was decided by the solid addition method [24].

2.3. Preparation of dye solution

Indigo Carmine ($C_{16}H_8N_2Na_2O_8S_2$ >99.9%) was purchased from Merck company. The concentration of IC dye obtained via UV-Visible spectrophotometric detector (Shimadzu, Kyoto, Japan) which was set at 215 nm defined the equilibrium concentration of the solution after adsorption process [25]. The indigo carmine dye concentration in each solution was determined by a UV-Visible spectrophotometric detector, which presented an uncertainty of less than ±3%.

2.4. Batch experiments

For calculating the capacity of the adsorbent and evaluation the isotherm models, batch adsorption process was performed by meeting 10 ml of IC dye solution in a separate flask containing 0.1 g nanoporous graphene as an adsorbent at ambient temperature. The flask was transferred to magnet stirrer shaken for 3 h to attain the equilibrium point. The adsorption time and dye initial concentration were varied from 0 to 150 min and 10 to 1000 ppm, respectively. The IC dye concentration in the solution after adsorption process was calculated by using UV-Visible spectrophotometer (model LAMBDA 750, Perkin Elmer) at the maximum absorption wavelength (λ_{max}) of 520 nm. The amount of IC dye retained in the adsorbent (q) was calculated by:

$$q_e = \frac{C_0 - C_e}{m} * V$$

where, C_0 and C_e present for the initial and the equilibrium concentration of IC dye, V is the volume of the solution (l) and m is the adsorbent mass (g).

2.5. Fixed bed adsorption experiment

The continuous experiments of the adsorptive IC dye removal were done by glass column with 10-28 cm length and Inner Diameter (ID) of 3 cm. The inlet flow rate of the solution was set 1 to 10 ml/min with the usage of peristaltic pump. The graphene nanoadsrobent was filled in the column and the solution was pumped upward through the column at a various flow rates (1, 5, 10 ml/min) at pH 9 using a peristaltic pump (Prominent, Heidelberg, Germany). The column bottom was fixed by a stainless steel sieve following by a layer of glass wool. The initial concentration of IC dye was studied in continuous removal system by fixed bed process varied from 10 to 100 ppm. The height of the adsorption column

was changed from 10 cm to 28 cm. In order to investigate the breakthrough curves of the adsorption process, the outlet dye concentration of the effluent (C_t) was calculated by UV-Visible spectra photometer. All the experiments were done at room temperature. The continuous fixed bed column schematic is clarified in Fig. 1.

The results of IC dye adsorption onto graphene in a continuous column were studied in the form of breakthrough curves which presented the behavior of the IC dye loaded to the adsorbent from the solution. The breakthrough curve was stated in terms of normalized concentration (the ratio of the outlet IC dye concentration to the inlet IC dye concentration) versus time (C_t/C_o vs. t). Effluent volume (V_{eff}) is achieved from Eq. (1).

$$V_{eff} = Q, t_{total} \tag{1}$$

where, t_{total} and Q are the total time of the continuous adsorption (min) and flow rate of the influent (ml/min), respectively. The treated water after adsorption was collected in a beaker. The dye concentration in the treated water (C_{wt}) can be calculated by the Eq. (2).

$$C_{wt} = \frac{\int_0^t C_t dt}{t} \tag{2}$$

The capability of the adsorbent was measured by adsorbent capacity (q). The adsorbent capacity was calculated from Eq. (3).

$$q = \frac{\rho_f V_{eff}}{1000, m_{ads}} \int_0^t \left(C_i - C_{(t)}\right) dt \tag{3}$$

where, q is adsorbent capacity (mg/g adsorbent), ρ_f is the density of dye solution (g/ml), V_{eff} is the dye solution flow rate (ml/min), m_{ads} is the mass of packed adsorbent (g), and C_i is the initial concentration of dye solution (ppm) [26].

In order to approve the repeatability of experiments, all the test was repeated and run twice.

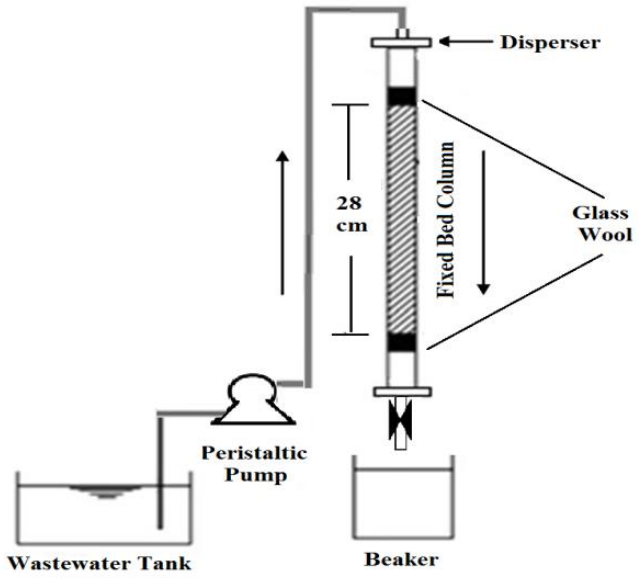

Fig. 1. The continuous fixed bed column system

2.6. Reusability and desorption studies

Regeneration process was performed to refresh the used adsorbents. The continuous desorption process was done by chemical washing. For this aim, HCl (0.1 M) as the desorbing solvent was pumped into the fixed-bed column packed with adsorbent saturated with the adsorbed dyes until the effluent concentration of dye was decreased near zero. The removal efficiency of the adsorbent was investigated after each regeneration cycle.

3. MATHEMATICAL MODELING

The assumptions of the fluid velocity and distribution of the solution concentration in the fixed bed column in the presence of adsorption under various process parameters investigation are as follow:

1. The neglect of the viscous force around the adsorbent in packed bed column flows is often acceptable.

2. The adsorbent in solid phase is determined to be a homogeneous and is packed uniformly through the column.

3. The equilibrium state between the solid phase (adsorbent) and liquid phase (the solution) assumes instantaneously.

These assumptions make the simulation simple and allow having a combined comprising equation for the solid and liquid phase.

3.1. Fluid dynamics

The fixed bed adsorption column performance of the fluid dynamics was simulated under the governing equation such as: Continuity and Navier–Stokes equations, which pose the Brinkman equations in porous medium. (Eqs. (4) and (5)):

$$\frac{\partial}{\partial t}(\varepsilon\rho) + \nabla\left(\rho\vec{U}\right) = 0 \tag{4}$$

$$\frac{\rho}{\varepsilon}\left[\frac{\partial \overline{U}}{\partial t} + \left(\overline{U}, \nabla\right)\frac{\overline{U}}{\varepsilon}\right] = -\nabla P + \nabla, \left[\frac{1}{\varepsilon}\left\{\mu\left(\nabla\vec{U} + \left(\nabla\vec{U}\right)^T\right) - \frac{2}{3}\mu\left(\nabla, \vec{U}\right)\right\}\right] - \left(\kappa^{-1}\mu\right)\vec{U} + F \tag{5}$$

In these equations [27], ε is the porosity of porous medium, ρ kg/m^3 and μ [kg/m.s] are the density and the dynamic viscosity of the fluid, respectively. Parameter, P is the pressure, U indicates the velocity vector, and F stands for the volume force of the regions. The term κ [m^2] is the permeability tensor of the porous medium that can be gained from Ergun's equation [28]:

$$\kappa = \frac{d_p{}^2 \varepsilon^2}{150(1-\varepsilon)} \tag{6}$$

where, ε and d_p show the porosity and particle diameters, respectively.

In computational fluid dynamics simulation process the IC concentration can be calculated at any time vs. place in the system during the whole adsorption process. This clearly depicts the limits of the analytical approach, which can be only explained for steady-state conditions.

3.2. Mass transfer

A convection–diffusion-adsorption-dispersion model is applied to compute the species concentration and transport in saturated porous media [28]:

$$\frac{\partial}{\partial t}\left(\varepsilon_p C_i\right)+\frac{\partial}{\partial t}\left(\rho_b C_{p,i}\right)+u,\nabla C_i=\nabla,\left[\left(D_{D,i}+D_{e,i}\right)\nabla C_i\right]+R_i+S_i \quad (7)$$

$$\rho_b=\left(1-\varepsilon_p\right)\rho \quad (8)$$

First two terms on the left side correspond to the accumulation of species within the liquid phase and solid phase, while the last term describes the convection because of the velocity field. In these equations, C_i denotes the concentration of species i in the liquid [mol/m^3], ε_p is the porosity, ρ_b [kg/m], ρ [kg/m] are the bulk density and solid phase density, respectively. $D_{e.i}$ [m^2/s] is fluid diffusion coefficient which is the expression for each species in fluid. The term $D_{D.i}$ [m] is the dispersion coefficient, u [m/s] stands for velocity field. The two last terms on the right-hand side describe production or consumption of the species i with R_i being the reaction rate and S_i the arbitrary source term that were neglected in this study. $C_{p.i}$ is the adsorbed amount of species on the solid phase. The Langmuir isotherm model was illustrated the dye equilibrium data in the solution and the solid phases and can be shown as [29]:

$$\frac{\partial C_{p,i}}{\partial C_i}=\frac{K_L\times C_{P\max}}{\left(1+K_{L,C}\right)^2} \quad (9)$$

where, K_L [mol/kg] is the Langmuir constant and C_{Pmax}

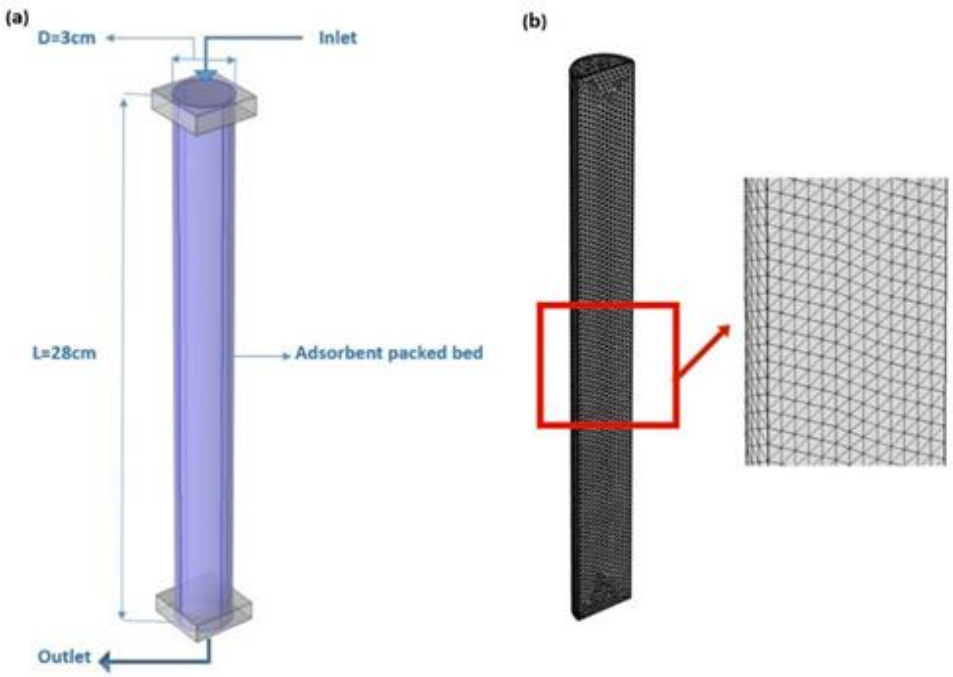

Fig. 2. (a) schematic drawing of packed bed column. (b) illustration of the mesh refining used in CFD simulations

Table 1. Grid independence verification

Average concentration at outlet per initial concentration	Number of elements in mesh
0.99	100496
0.985	84700
0.998	80470
0.952	73037
0.932	70050
0.89	67520

[mol/kg] represents the maximum adsorption.

3.3. Numerical solution

In this research, the adsorption packed bed column was simulated three-dimensionally by COMSOL Multiphysics version 5.3a. The complete packed bed column was built in the CFD geometry (Figs. 2(a) and 2(b)). Due to symmetry, for the analysis only half of the geometry was deliberated. Thus, only half of the geometry was meshed in order to reduce computational time and the run time. An impression of the computational grid is depicted in Fig. 2(b). In order to get grid independent results, six grids having different meshes of 67520- 100496 were examined. The number of elements size was listed in Table 1. Triangular cells were used for refining at the boundaries, inlet, and outlet of the column. As a result, the mesh numbers of 80407 grids were used for generating the results. The physical properties of the fluid, porous medium and parameters are summarized in Table 2 [30]. The used boundary conditions set for solving the model equations are summarized in Table 3. However, dispersion coefficient values were estimated at the desired flow rate. Permeability was obtained from Ergun's equation [31]. Effective mass diffusion coefficient can be obtained from Millington and Quirk model [32]. The constant parameters of Langmuir isotherm model were calculated from batch experimental adsorption process. Additionally, the governing equations of steady-state flow coupled with the time-dependent transport equation in order to calculate the advection, diffusion, and adsorption capacity of synthesized adsorbent through the fixed bed column. The tolerance (relative) 0.001 in time-dependent solver was satisfied as a convergence criterion.

4. VALIDATION

Comparing the results with the experimental data was called the validation of the simulation. Brinkman equations in porous medium model were used to simulate the steady-state laminar flow profile at 1 ml/min for the packed bed, as shown in Fig. 3. In order to compare the local differences, the velocity was set manually in the range of 0–0.006 m/s.

Fig. 4 depicts a comparison of the simulation outcomes with experimental data for the breakthrough curve at 1 ml/min, concentration of 10 ppm and a bed height of 24 cm. It is concluded from validation test that the modeling methodology is quite consistent, concluded that the coupling between complex physics, and the achieved parameters can be prepared to predict the breakthrough curve under different conditions.

5. RESULT AND DISCUSSION

5.1. Characterization of synthesized adsorbent

The XRD pattern of the prepared nanoadsorbent is obtainable in Fig. 5. Because of the intrinsic nature of graphene, the pattern of the synthesized graphene is similar to graphite . It is clear in Fig. 5, that the strong peaks at 2θ of 26.80° and 27.10° are the characteristic peaks of synthesized graphene [33]. The XRD pattern results indicate that the nanostructure graphene synthesized via CVD method has a single layer [34].

SEM image of the synthesized sample is displayed in Fig. 6. As can be seen, graphene has been formed uniformly through the synthesis process. A highly porous media with small pore size is exhibited in the Figure.

Fig. 7(a) displays the nitrogen adsorption/desorption

Table 2. Physical parameters of fluid and porous medium used in the CFD simulations

Parameter	Value	
ρ_b	700 [kg/m^3]	The density of fluid
ρ	400 [kg/m^3]	Solid phase density
μ	0.003 [Pa.s]	The fluid dynamic viscosity
ε_p	0.3	The porosity of porous medium
κ	1.3×10^{-6} [m^2]	Permeability
d_p	25 [μm]	Particle diameter

Table 3. Boundary conditions in fluid phase.

Boundary condition		
Position	Flow modeling	Mass modeling
inlet	Fully developed laminar flow	Constant dye concentration
Outlet	Pressure outlet	convection and adsorption
Wall	No- slip condition	Zero mass flux
Initial condition		
t=0		C_0=0

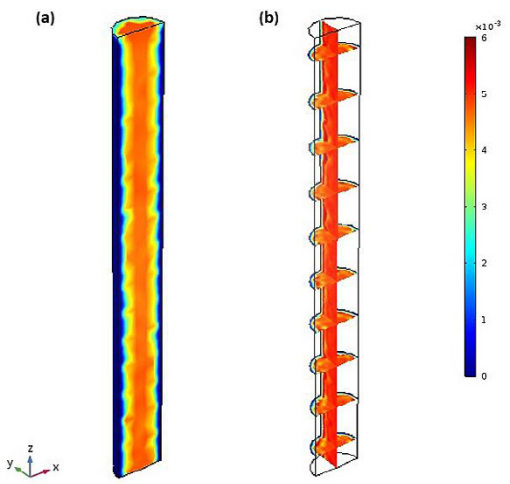

Fig. 3. (a) Velocity magnitude field (m/s) for the packed bed column of the adsorption process. (b) Contours of velocity magnitude on longitudinal and transverse planes for steady-state flow (effluent flow rate 1 ml/min).

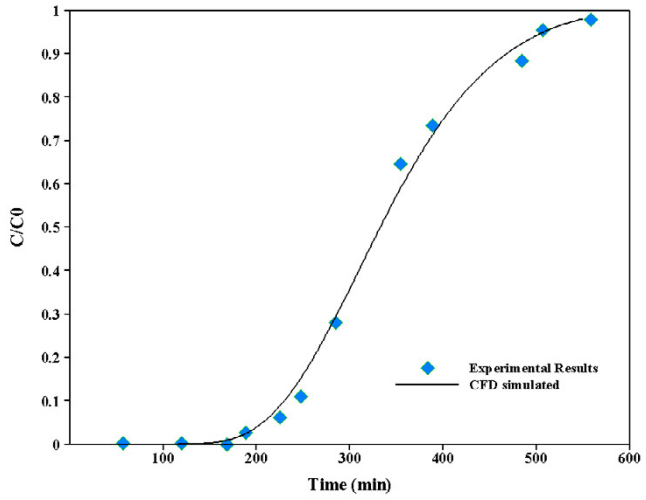

Fig. 4. Comparison of the simulation results with experimental data for breakthrough curve

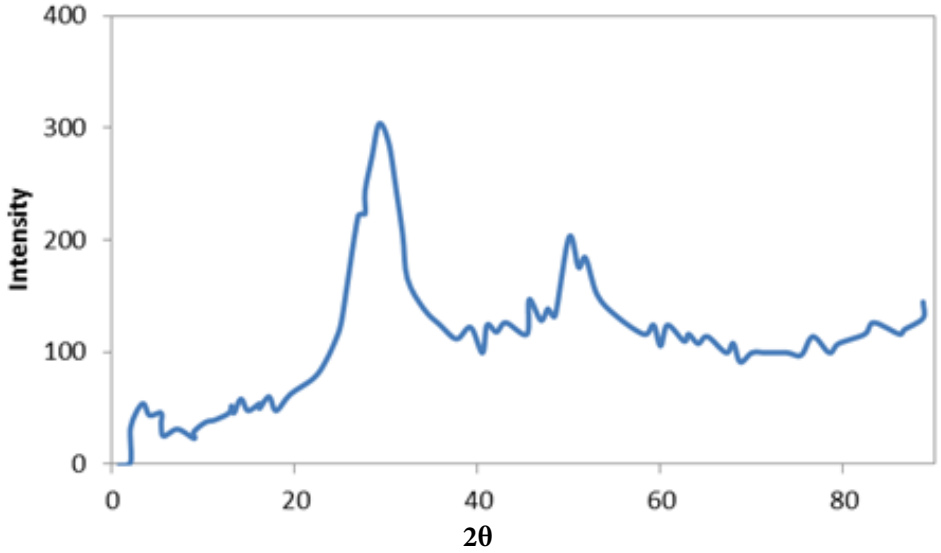

Fig. 5. XRD pattern of the synthesized nanostructure graphene

isotherm. It is evident that the behavior of synthesized graphene corresponds to type 4 which designate the formation of mesoporous structure with pore diameter from 2 to 50 nm range. As Fig. 7(b) shows, the main pore size corresponded to mesoporous materials and proved that the synthesized graphene is in the nanoporous group [35]. In addition, the total pore volume of the synthesized graphene is 2.01 cm^3/g at relative pressure (P/P_0) of 0.98. The considered BET surface area, pore size, and pore volume of graphene are defined in Table 4. Due to the high surface area and high pore volume which is concluded from the results the synthesized graphene has a good capability for the adsorption process.

Also the main elements in the structure of graphene are detected by elemental analysis (CHN) which the results are reported in Table 5.

5.2. Isotherm modeling

The effect of IC dye initial concentration was evaluated in various amounts from 10 to 100 ppm in a batch series experiments. The adsorption capacity is increased, because of the low driving force at low liquid concentrations. Principally this can be clarified by obtainable active sites. At low adsorbate concentration, the ratio of surface active sites to IC dye molecules is high. The Langmuir and Frendiulich isotherm models were used to consider the adsorptive capacity and similarity of adsorbent . The parameters of the isotherm models are summarized in Table 6. The regression coefficient values (R^2) demonstrate that Langmuir model is more suiTable to fit the equilibrium data. The assumption of Langmuir model describes that each physical and chemical adsorption equilibrium at the irregular homogenous adsorption sites on the solid surface [36,37].

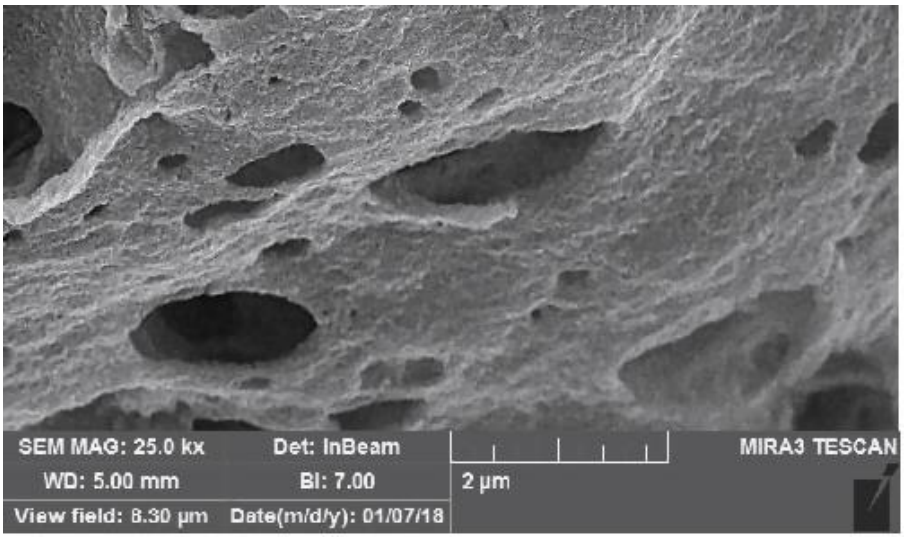

Fig. 6. The SEM image of the synthesized graphene

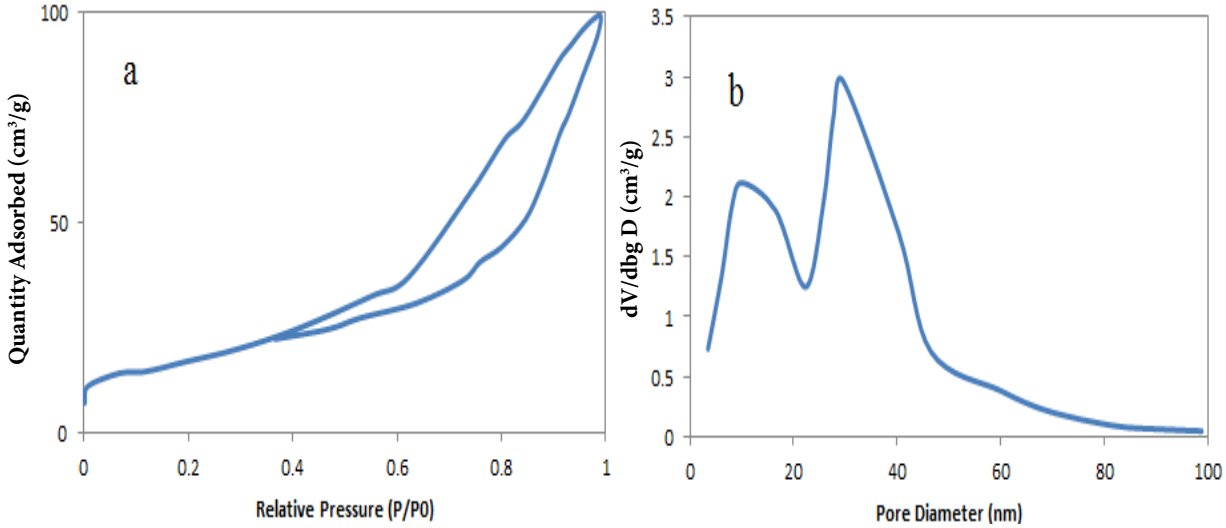

Fig. 7. (a) The N_2 adsorption isotherm at 77 K on nanoporous graphene, (b) The pore size distribution of high surface area nanoporous graphene.

5.3 Kinetic modeling

The adsorption process procedure is understood from kinetic modeling data. The adsorption process rate-controlling step and the uptake rate of dye were studied the utilization of various kinetics models (i.e., first-order, pseudo-second-order, and intraparticle models). The adsorption data was demonstrated that adsorption rate was followed by the second-order model. According to Table 7, from the regression coefficient (R^2) became 1.0, it can be concluded that the kinetic data were fitted by pseudo-second-order adsorption model better than the pseudo-first-order model. It is obvious from Table 7; the calculated values of q_e were in good agreement with the values obtained from experiments. Also the rate-limiting step of the IC dye adsorption is checked by an intraparticle model. The second section with light slope refers to the intraparticle diffusion which controls the adsorption process [38,39].

5.4. Effect of the solution flow rate

The effect of adsorbent performance in the continuous adsorption column was studied by considering the effect of solution flow rate on the adsorption. To confirm the convection–diffusion-adsorption-dispersion model the results of the simulation section were compared with the experimental BreakThrough Curves (BTC) data.

Three different flow rates were studied with a constant bed height of 24 cm and inlet IC dye adsorbate concentration of 10 ppm, as shown by the experimental breakthrough curves and CFD model results in Fig. 8. The comparison of breakthrough curves at different flow rates indicates that the maximum capacity of IC dye adsorption on the graphene occurs at the lower flow rate. The removal efficiency of the IC dye was

Table 4. N_2 adsorption data of synthesized nanostructure graphene

Sample	BET surface area (m^2/g)	Total pore volume (cm^3/g)	Pore size (A^0)
Graphene	971	2.01	90.1

Table 5. Elemental Analysis of the synthesized graphene

Sample	Carbon (wt %)	Hydrogen (wt %)
Graphene	99.2	0.8

Table 6. The equilibrium constants of adsorption isotherms

Isotherm model			
Langmuir	Q_0	k_l	R^2
	538.9	4.21×10^{-2}	0.989
Freundlich	n	k_F	

Table 7. Kinetic model parameters for the adsorption of IC dye onto graphene

Kinetic model	parameters		$q_{experimental}$	Regression Coefficient
	q_e (mg/g)	K_1 (mg/g.min)	q_{exp} (mg/g)	R^2
Pseudo first order	40.1	3.1×10^{-2}	81.4	0.74
Pseudo second order	82.1	4.1×10^{-3}	81.4	1.0
Intra particle Diffusion	K_I	C	--	
Step 1	6.01×10^{-1}	59.8	--	0.98

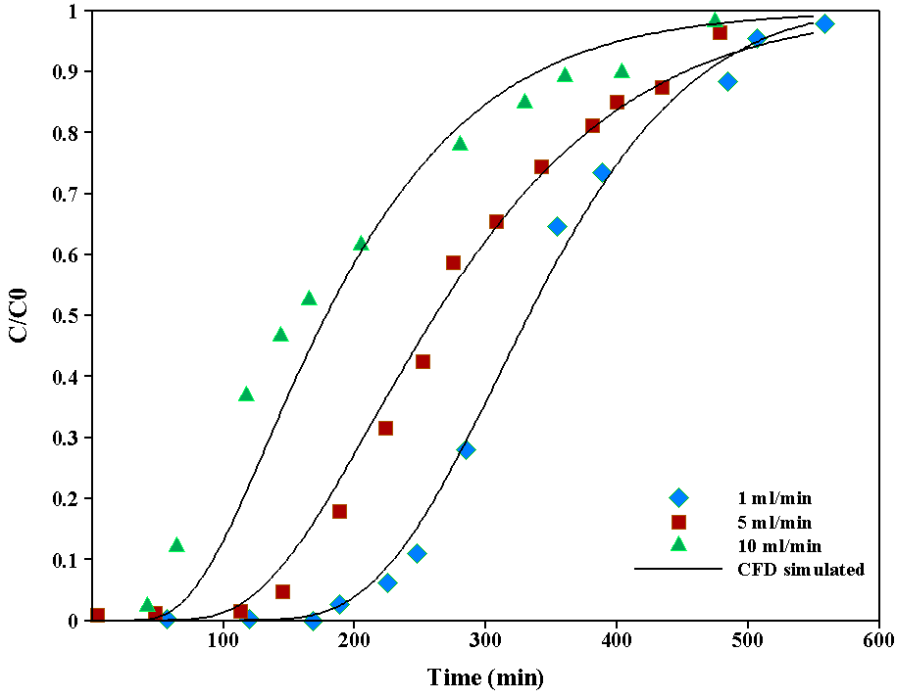

Fig. 8. Breakthrough curves at different flow rate of IC dye onto graphene nanoadsorbent.

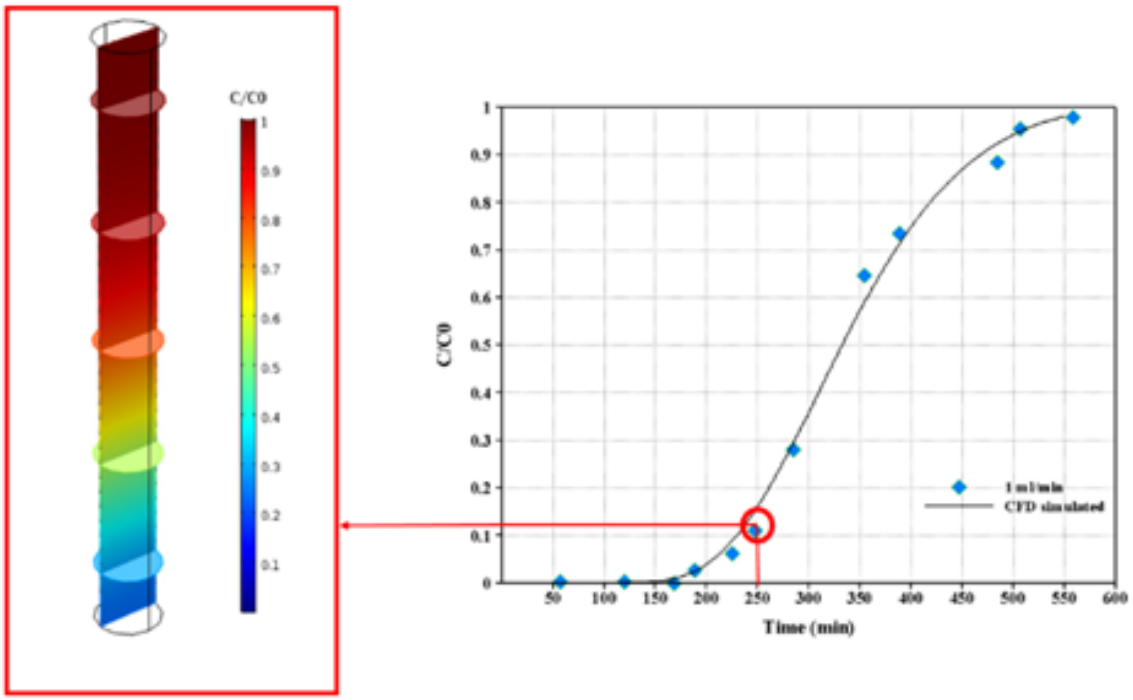

Fig. 9. CFD simulated IC concentration profile throughout the packed bed adsorption column vs. Experimental breakthrough curves (conditions: initial dye concentration 10 ppm at last time, IC dye flow rate = 1 ml/min, bed height = 28 cm, time =250 min).

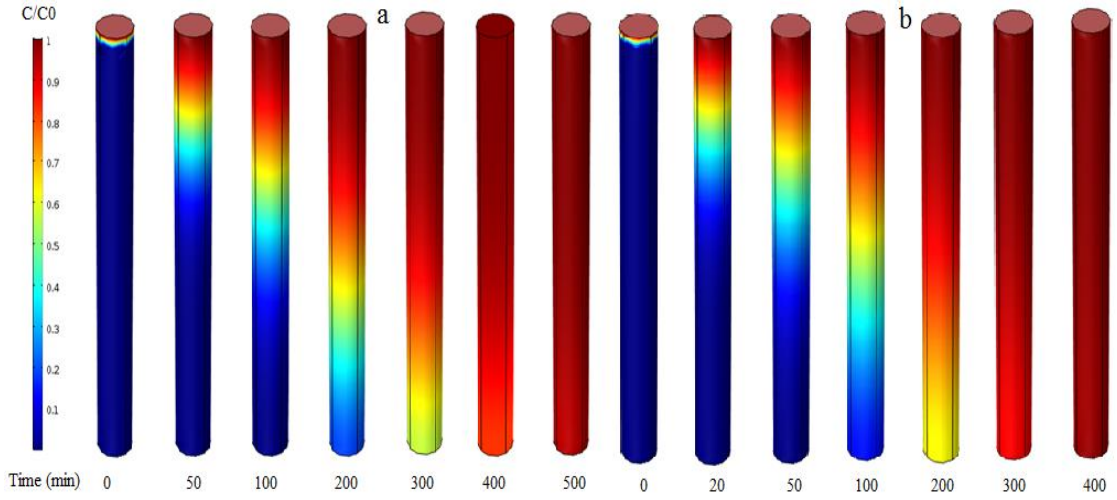

Fig. 10. Simulated contours of mass transfer rate obtained as a function of the adsorption (conditions: IC dye concentration 10 ppm at last time, bed height = 28 cm) a) IC dye flow rate = 5 ml/min, b) IC dye flow rate = 10 ml/min.

increased from 51% to 67% as flow rate decreased from 10 ml/min to 1 ml/min. The experimental data are summarized in Table 8 which proves that with increasing the flow rate, the removal efficiency decreases. Due to the insufficient time of IC dye mass transfer, the removal efficiency decreases with increasing flow rate. At high flow rate experiments (short breakthrough time), the durability of the dye solution is short and the adsorbate molecules do not have enough time to diffuse into the pores of the adsorbents [40]. By increasing the flow rate, the break time declines and the breakthrough curve gets sharper. In the higher flow rates, the IC dye molecules do not have enough time to penetrate in to the adsorbent pores and the concentration of IC dye at the front of the mass transfer zone have not sufficient time to reach the equilibrium concentration, so the effluent solution leaves the column without diffusion [41].

In Fig. 9 the adsorptive removal of the IC dye solution was shown via CFD simulation. With the aid of CFD simulation, the dye concentration at adsorbent and adsorbate can be obtained at any given time, at any given location in the system throughout the entire dye removal adsorptive process. This descripts the limits of the analytical solution, which can only

Table 8. The experimental data of the adsorption column with different flow rate

Flow rate (ml/min)	Bed height (cm)	Concentration (ppm)	Breakthrough time (min)	Adsorption capacity (mg/g)
1	28	10	223	167
5	28	10	156	208
10	28	10	87	349

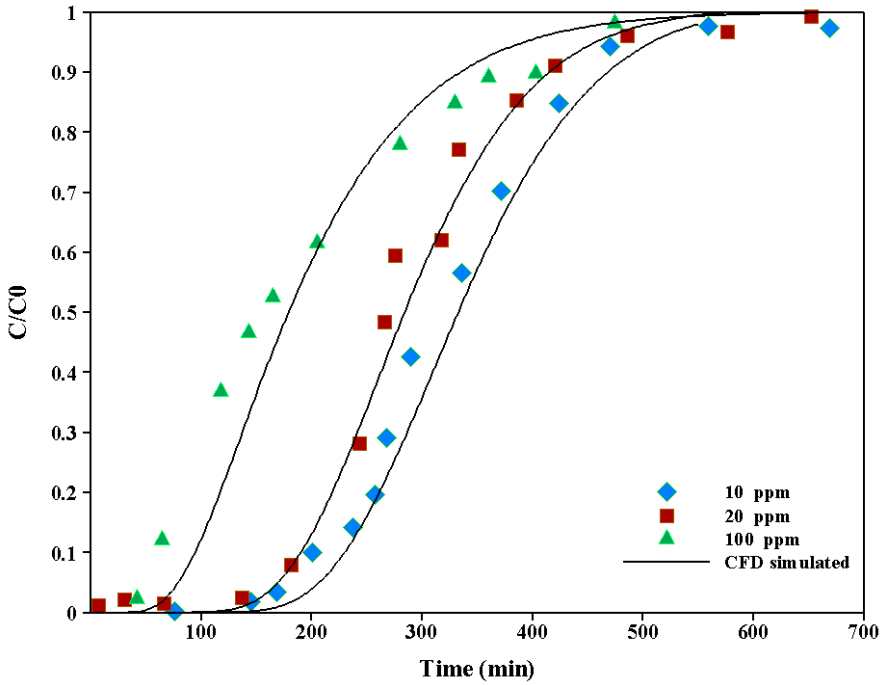

Fig. 11. Breakthrough curves at different initial concentration of IC dye onto graphene nanoadsorbent

account for steady state situations. Therefore, the flow rate of 1 ml/min (in the conditions under study), which was chosen as the optimized operating parameter, was used to study the influence of initial concentration on BTC.

The data in Table 8 demonstrate that the increase of the flow rate causes the reduction of the dye removal efficiency. The breakthrough times increase from 87 min to 223 min as the flow rates increase from 1 to 10 ml/min (Table 8). The mass transfer fundamentals can describe the variation of the breakthrough curve slope and adsorption capacity [42].

Fig. 10 shows that The IC concentration profile throughout the column as a function of time and influence the break-point and saturation time. Modeling showed that breakthrough curves was influenced by the properties of the compound, the porosity of porous medium, particle diameter of adsorbent. It can be concluded from the experiments that, the adsorption capacity of the adsorbent in the fixed bed column appearance decreased, subsequent in lower local mass transfer rates.

5.5. Effect of initial dye concentration

To study the dye concentration effect on the adsorption process parameters column, the concentration was changed from 10 to 100 ppm. The experiment is performed at bed height of 28 cm and flow rate of 1 ml/min. The initial IC dye concentration changes influence the breakthrough curve. The effect of the inlet IC dye concentration on the experimental BTC and CFD simulated values are investigated which are shown in Fig. 11. The breakthrough curves determine that as the initial dye concentration rises breakthrough time and saturation time decrease. The increase of initial concentration of IC dye augmented the concentration gradients and caused the higher mass transfer rates. In addition, it is resulted from Fig. 11 that the adsorption process up to the break point (about 233 min) was controlled via fluid phase convection and the diffusion inside the particles pores.

The removal efficiency of dye adsorption is lower than batch experiments range, because the dye molecules do not have enough time to contact with the adsorbent site so some molecules left the adsorption column unabsorbed [43,44].

Fig. 12 show IC concentrations profile throughout the packed bed adsorption column as a function of time. As earlier discussed, the adsorption rate was relative to the inlet IC dye concentration. As Fig. 12 depicts, the bed saturation occurred gradually as the mass transfer zone proceeded through the bed [45]. The results of the experimental data are shown in Table 9. It is evident from Table 9 that the capacity

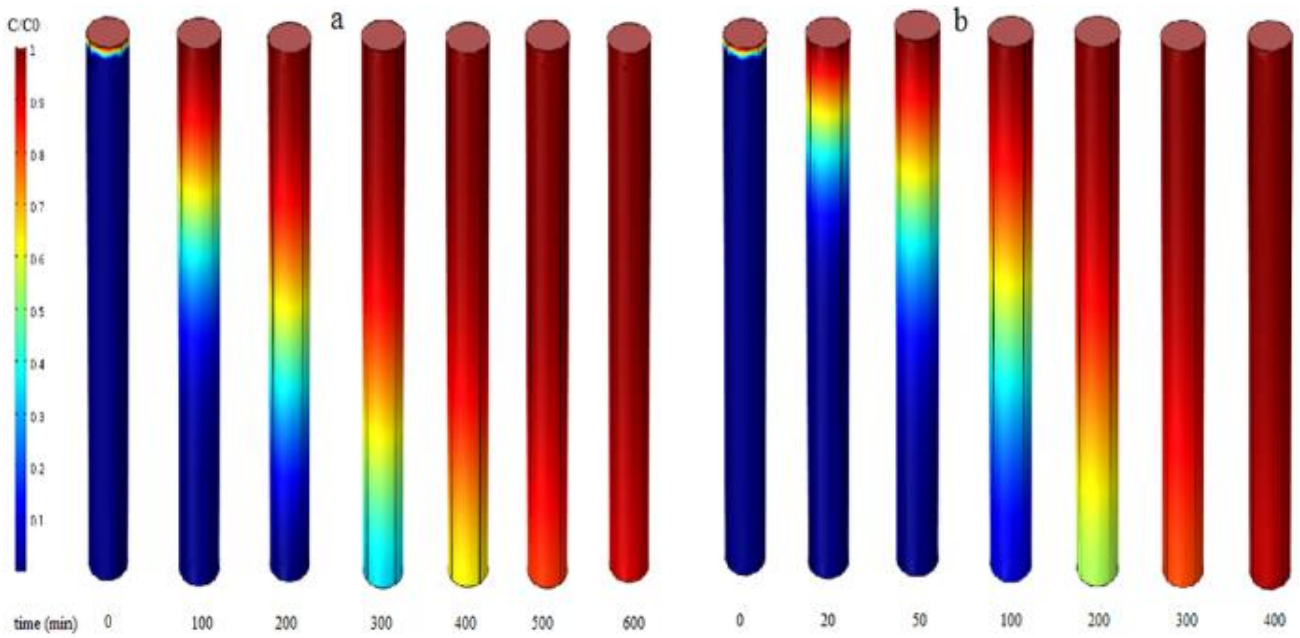

Fig. 12. Simulated contours of the adsorption conditions such as mass transfer rate: IC dye flow rate = 1 ml/min, bed height = 28 cm a) initial dye concentration 10 ppm, b) initial dye concentration 100 ppm.

Table 9. The experimental data of the adsorption column with different dye concentration

Flow rate (ml/min)	Bed height (cm)	Concentration (ppm)	Breakthrough time (min)	Adsorption capacity (mg/g)
1	28	10	223	167
1	28	50	191	195
1	28	100	43	286.3

of the adsorption process increases with increasing the dye concentration from 10 to 100 ppm.

Due to a decreased diffusion coefficient or decreased mass transfer coefficient the lower concentration gradient caused a slower flux of the mass transfer [46]. The initial dye concentration is varied from 10 ppm to 100 ppm therefore the adsorption capacity of graphene augmented from 167 mg/g to 286.3 mg/g. The driving force of the adsorptive IC dye removal is enhanced by the increasing of the initial dye concentration. These conclusions are affirmed the results of the literature reviews [47].

5.6. Effect of adsorbent bed height

The effect of bed height on IC adsorptive removal was evaluated at different heights of 10 to 28 cm with a constant initial concentration of 10 ppm and flow rate of 1 ml/min. In order to inaugurate the optimum performance of the continuous fixed-bed system, the bed depth effect on the breakthrough time is evaluated. Fig. 13 demonstrate the performance of breakthrough curves and CFD model result at bed heights of 10, 15, 28 cm. The IC concentration profile throughout the fixed bed column is shown in Fig. 14 as a function of time until the saturation time. The bed height evaluation results of IC dye removal are summarized in Table 10. As results emphasize, with the increase of bed depth, the breakthrough time is increased from 78 to 591 min. This comparison is explained by the fact that the increase of the bed height causes the enhancement of the contact time and the IC dye molecules have sufficient time to diffuse into the adsorbent sites.

The resistance time of the adsorbate in the continuous column is enhanced by growing the bed height. The breakthrough time plays an important role in determining the parameters of the adsorption process. According to the batch experimental results by increasing the breakthrough time the intraparticle diffusion mass transfer mechanism become important therefore, high breakthrough time causes higher adsorption capacity in continuous system [48-50]. Due to the resistance time increase of IC dye solution, the adsorption capacity of the graphene increased from 129.2 to 357.1 mg/g by increasing the bed height of the adsorption column from 10 to 28 cm. This can be attributed to the fact that more binding site is available in the highest bed depth [51].

6. REUSABILITY AND DESORPTION STUDIES

Regeneration process was performed to refresh the used

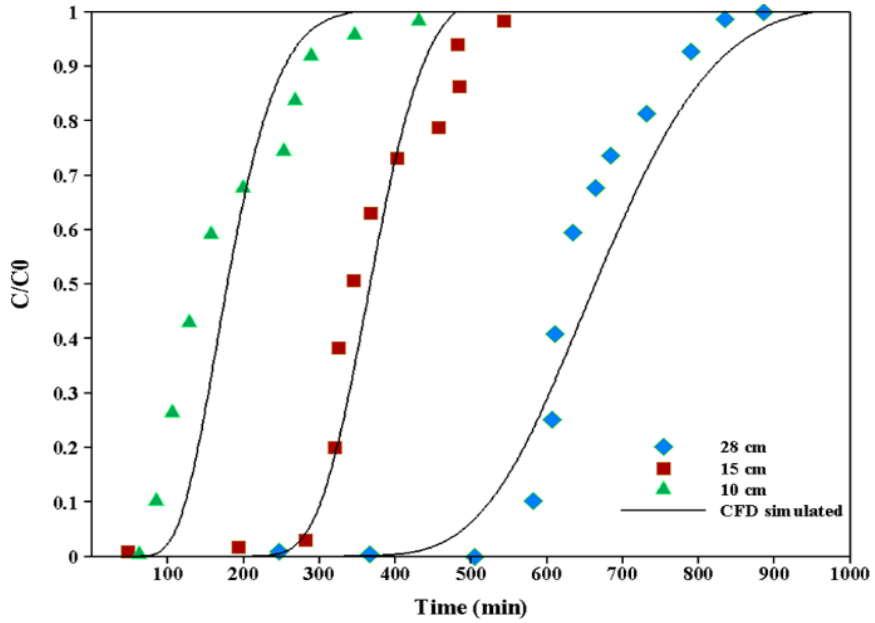

Fig. 13. Breakthrough curves at different bed height

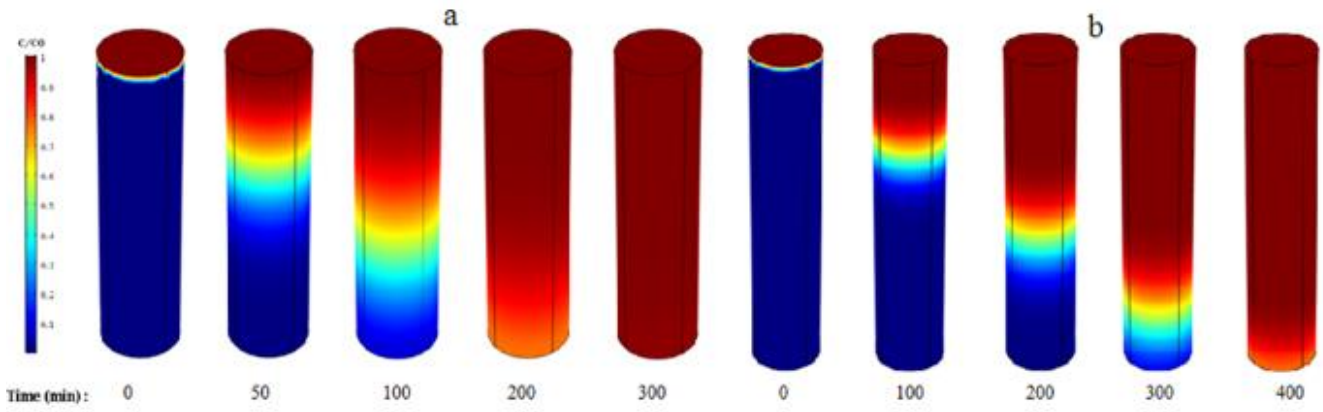

Fig. 14. Simulated contours of mass transfer rate obtained as a function of the adsorption (conditions: IC dye concentration 10 ppm at last time, IC dye flow rate =1 ml/min) a) bed height = 10 cm, b) bed height = 15 cm

Table 10. The experimental data of the adsorption column with different bed height

Flow rate (ml/min)	Bed height (cm)	Concentration (ppm)	Breakthrough time (min)	Adsorption capacity (mg/g)
1	10	10	78	129.2
1	15	10	298	201.8
1	28	10	591	357.1

adsorbents. The continuous desorption process was done by chemical washing method. For this aim, the HCl (0.1 M) as a desorbing solvent was drained into the packed column with adsorbed dyes until the effluent concentration of dye was gained nearly zero. The removal efficiency of the adsorbent was investigated after each regeneration cycle [52,53]. The removal efficiency vs. regeneration recycles is plotted in Fig. 15. It is obvious from Fig. 14 that after six cycles, removal efficiency of the regenerated adsorbent was decreased about 20%. This study shows that graphene is a potential adsorbent for water purification.

The improving of the dye sorption process was resulted

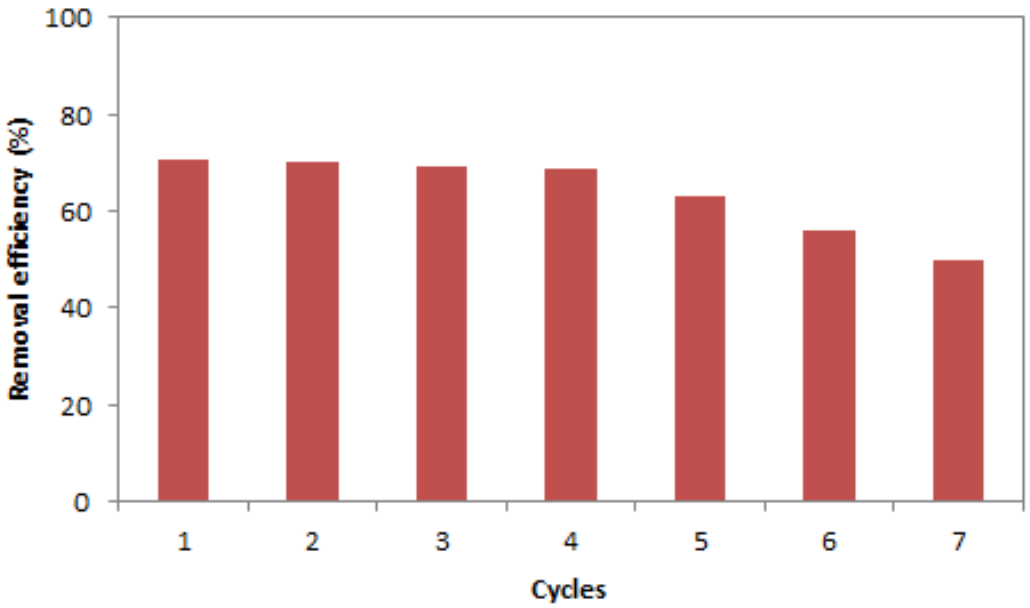

Fig. 15. Comparison of regeneration cycles and removal efficiency

Table 11. Comparison of sorption capacity and removal efficiency of dye by different adsorbents

Adsorbent	Adsorbent capacity (mg/g)	Removal efficiency (%)	References
Activated carbon	65	63	[49]
Poly (acrylic acid)/MnFe2O4	53	57	[50]
Raw kaolin	26	43	[51]
Chitosan/zeolite	24	42	[52]
Sodium montmorillonite	42	53	[53]
Nano porous graphene	82	78	This work

that the maximum adsorption capacities of IC dye on the synthesized adsorbent was gained 82 mg/g, respectively, which was higher than the literature review in Table 11. Due to the nanostructure, porosity and large surface area of the adsorbent as previously shown in Fig. 6 the huge dye adsorption capacity of the synthesized adsorbent was concluded.

7. CONCLUSION

The CFD simulation data proved to be accurate and indicated that CFD is potential software to fit and evaluate all relevant IC dye adsorption results onto the nanoporous graphene. Results indicated that CFD can represent the adsorption data of IC dye onto graphene as a function of time and location, both in the bulk and on the surface. In order to confirm the experimental data, the results of the simulation were compared with experimented breakthrough curves achieved for various adsorption process conditions (flow rate, initial dye concentration and bed depth). The breakthrough curves experiments were studied at different flow rates, initial dye concentrations and bed height at 25 ^{0}C. According to the experimental results, the optimized process parameters were determined as follows: a flow rate of 1 ml/min, a packed bed length of 28 cm and an IC dye initial concentration of 10 ppm. The IC dye removal efficiency of the fixed bed column onto the nanoporous graphene as the adsorbent was about 67% at optimized condition of the adsorption process. The decrease of the total dye removal uptake adsorption capacity is determined by increasing the inlet flow rate. The decrease of the bed depth persuaded the breakthrough curves sharper. The CFD results were fitted to experimental continuous results which for different inlet flow rates, IC dye concentrations, and packed bed depth in order to confirm the model. The convection of the fluid phase and the diffusion within the adsorbent pores were the controlling mechanism of the adsorption process until the system attained the break point. The regeneration tests confirmed that nanoporous graphene adsorption capacity decreased about 20% after six cycle regeneration.

REFERENCES

[1] M. Bahgat, A. A. Farghali, W. M. A. El.Rouby, M. H. Khedr. Synthesis and modification of multiwalled carbon nanotubes (MWCNTs) for water treatment applications, *Journal of Analytical and Applied Pyrolysis*. 92 (2011) 307–313.

[2] A. Gucek, S. Sener, S. Bilgen, M. Mazmanci. Adsorption and kinetic studies of cationic and anionic dyes on pyrophyllite from aqueous solutions, *Journal of Colloid and Interface Science*. 286 (2005) 53–60.

[3] L. L. P. Lim, R. J. Lynch, S. I. In. Comparison of simple and economical photocatalyst immobilisation procedures, *Applied Catalysis A: General*. 365 (2009) 214–221

[4] R. Rehman, J. Zafar, H. Nisar, Adsorption studies of removal of indigo carmine dye from water by formaldehyde and urea treated cellulosic waste of citrus reticulata peels, *Asian Journal of Organic Chemistry*, 26 (2014) 43–47.

[5] G. Z. Kyzas, P. I. Siafaka, E. G. Pavlidou, K. J. Chrissafis, D. N. Bikiaris, "Synthesis and adsorption application of succinyl-grafted chitosan for the simultaneous removal of zinc and cationic dye from binary hazardous mixtures, *chemical Engineering journal.* 259 (2015) 438–448.

[6] A.K. Giri, T.S. Banerjee, G. Talukder, A. Sharma, Effects of dyes (indigo carmine, metanil yellow, fast green FCF) and nitrite in vivo on bone marrow chromosomes of mice, *Cancer Letters*. 30 (1986) 315–320.

[7] E. Ojuz, B. Kesanikar, Z. Celik, Ozonation of Aqueous Bomplex Red CRL dye in a Sami batch reactor, *Dyes and pigment*. 64(2) (2005) 101-108.

[8] O.T. Can, M. Kobya, E. Demirbs, M. Bayronoglu, Treatment of the textile waste water by combined electro coagulation, *Chemosphere journal*. 62 (2006) 181-187.

[9] P. Daraei, S.S. Madaeni, N. Ghaemi, M. AliKhadivi, B. Astinchap, R. Moradian. Enhancing antifouling capability of PES membrane via mixing with various types of polymer modified multi-walled carbon nanotube, *Journal of Membrane Science*. 444 (2013) 184–191.

[10] A.H. Gemeay, I.A. Mansour, R.G. El-Sharkawy, A.B. Zaki. Kinetics and mechanism of the heterogeneous catalysed oxidative degradation of indigo carmine, *Journal of Molecular Catalysis A: Chemical.* 193 (2003) 109–120.

[11] V.L. Grimau, M.C. Gutierrez, 2006, Decolourization of simulated reactive dye bath effluents by electrochemical oxidation assisted by UV light, *Chemosphere Journal*. 62 (2006) 106–112.

[12] M.I. Banat, P. Nigam, D. Singh, R. Marchant. Microbial decolorization of textile-dye-containing effluents: A review, *journal of Bioresource Technology*. 58 (1996) 217–227.

[13] K.G. Bhattacharyya, A. Sharma. Adsorption characteristics of the dye, brilliant green, on neem leaf powder, *Dyes and Pigments*. 57 (2003) 211–222.

[14] O. Abdelwahab, A. El Nemr, A. El-Sikaily, A. Khaled. Biosorption of direct yellow 12 from aqueous solution by marine green algae Ulva Lactuca, *Journal of Chemical Ecology*. 22 (2006) 253–266.

[15] D. Mohan, K.P. Singh, G. Singh, K. Kumar. Removal of dyes from wastewater using flyash, a low cost adsorbent, *Industrial & Engineering Chemistry Research.* 41 (2002) 3688–3695.

[16] Z. Hosseini Dastgerdi, V. Abkhiz, S. S. Meshkat, N, Ghorbani. Preparation of novel magnetic grafted raft agent nanocomposite: Application in carmine dye adsorptive removal from waste water, *journal of Environment and Chemical Engineering.* 7 (2019)103–109.

[17] S. S. Meshkat, O. Tavakoli, A. M. Rashidi, M. D. Esrafili. Adsorptive mercaptan removal of liquid phase using nanoporous graphene: Equilibrium, kinetic study and DFT calculations, *Ecotoxicology and Environmental Safety*. 165 (2018) 533–539.

[18] A. M. Rashidi, M. M. Akbarnejad, A. A. Khodadadi, Y. Mortazavi, A. Ahmadpour. Single-wall carbon nanotubes synthesized using organic additives to Co–Mo catalysts supported on nanoporous MgO, *Nanotechnology* .18 (2007) 315605-315610.

[19] T. S. Singh, K. K. Pant, Experimental and modelling studies on fixed bed adsorption of As(III) ions from aqueous solution, *Separation and Purification Technology 48 (2006) 288-296*.

[20] M. Banerjee, N. Bar, R. K. Basu, S. K. Das. "Removal of Cr (VI) from Its Aqueous Solution Using Green Adsorbent Pistachio Shell: a Fixed Bed Column Study and GA-ANN Modeling, *Water Conservation Science and Engineering.* (2017) DOI:10.1007/s41101-017-0039-x.

[21] M. G. A. Vieira, A. F. Almeida Neto, M.L. Gimenes, M. G. C. Silva. Sorption kinetics and equilibrium for the removal of nickel ions from aqueous phase on calcined Bofe

bentonite clay, *Journal of Hazardous Materials*. 177 (2010) 362–371.

[22] N. Mohammed, N. Grishkewich, H. A. Waeijen, R. M. Berry, K. C. Tam, Continuous flow adsorption of methylene blue by cellulose nanocrystal-alginate hydrogel beads in fixed bed columns, *Carbohydrate Polymers.* 136 (2016) 1194-1202.

[23] S. H. Abdel-Halim, A. M. A. Shehata, M. F. El-Shahat. Removal of lead ions from industrial waste water by different types of natural materials. *Water Resource.* 37 (2003) 1678–1683.

[24] M. Jerold, Daisy Joseph, N. Patra, V. Sivasubramanian. Fixed-bed column studies for the removal of hazardous malachite green dye from aqueous solution using novel nano zerovalent iron algal biocomposite. *Nanotechnology for Environmental Engineering.*1 (2016) 7-17.

[25] M. Mukhopadhyay, S. B. Noronha, G. K. Suraishkumar Copper biosorption in a column of pretreated Aspergillus niger biomass, *Chemical Engineering Journal.*144 (2008) 386–90.

[26] Z. Al-Qodah, W. Lafi, 2003, Continuous adsorption of acid dyes in fixed beds, *Journal of Water Supply: Research and Technology.* 52 (2003) 189–98.

[27] C. A. d. Rosa, I. C. Ostroski, J. G. Meneguin, M. L. Gimenes, M. A.S.D. Barros. Study of Pb^{2+} adsorption in a packed bed column of bentonite using CFD, *Applied Clay Science.* 104 (2015) 48–58.

[28] S.W. Verbruggen, S. Lenaerts, S. Denys. Analytic versus CFD approach for kinetic modeling of gas phase photocatalysis, *Chemical Engineering journal*. 262 (2015) 1–8.

[29] J. Bear. Dynamics of Fluids in Porous Media; Dover Publications: Mineola, NY, 1988.

[30] A.A. Ahmad, B.H. Hameed, Reduction of COD and colour of dyeing effluent from a cotton textile mill by adsorption onto bamboobased activated carbon, *Journal of Hazardous Materials.* 172 (2009) 1538–1543

[31] T. Belin, F. Epron, Characterization methods of carbon nanotubes: a review, *Materials Science and Engineering: B*. 119 (2005) 105-118.

[32] R. J. Millington, J. P. Quirk, 1961, Permeability of porous solids, *Journal of the Chemical Society, Faraday Transactions,* 57 (1961)

1200–1207.

[33] C. N. R. Rao, B. Kanishka, K. S. Subrahmanyam, A. Govindaraj. Graphene, the new nanocarbon, *Journal of Materials Chemistry A*. 19 (2009) 2457–2469.

[34] R. JabariSeresht, M. Jahanshahi, A. M. Rashidi, A. A. Ghoreyshi. Synthesize and characterization of graphene nanosheets with high surface area and nanoporous structure, *Applied Surface Science*. 276 (2013) 672–681.

[35] E. Ghasemy, H. B. Motejadded, A. rashidi, T. Hamzehlouyan, Z. Yousefian. N-doped CNT nanocatalyst prepared from camphor and urea for gas phase desulfurization: Experimental and DFT study, *Journal of the Taiwan Institute of Chemical Engineers*. 85 (2018) 121–131.

[36] Z. Aksu, F. Gonen, Biosorption of phenol by immobilised activated sludge in a continuous packed bed: prediction of breakthrough curves, *Process Biochemistry.*39 (2004) 599–613.

[37] D. Charumathi, N. Das. Packed bed column studies for the removal of synthetic dyes from textile wastewater using immobilised dead, *C. tropicalis. Desalination*. 22 (2012) 30-285

[38] V. K. Gupta, B. Gupta, A. Rastogi, S. Agarwal, A. Nayak. A comparative investigation on adsorption performances of mesoporous activated carbon prepared from waste rubber tire and activated carbon for a hazardous azo dye – Acid Blue 113, *Journal of Hazardous Materials.*186 (2011) 891–901.

[39] M. Mukhopadhyay, S. B. Noronha, G. K. Suraishkumar. Copper biosorption in a column of pretreated Aspergillus niger biomass, *Chemical Engineering Journal*. 144 (2008) 386–390.

[40] R. Han, Y. Wang, W. Yu, W. Zou, J. Shi, H. Liu. Biosorption of methylene blue from aqueous solution by rice husk in a fixed-bed column, *Journal of Hazardous Materials*. 141 (2007) 713–718.

[41] S. Figaro, J.P. Avril, F. Brouers, A. Ouensanga, S. Gaspard. Adsorption studies of molasse's wastewaters on activated carbon: Modelling with a new fractal kinetic equation and evaluation of kinetic models, *Journal of Hazardous Materials.* 161 (2009) 649–656.

[42] J. Barron-Zambrano, A. Szygul, M. Ruiz, A.M. Sastre, E. Guibal. Biosorption of Reactive Black 5 from aqueous solutions by chitosan: column studies, *Journal of Environmental Management.*. 91 (2010) 2669–2675.

[43] C. A. d. Rosa, I. C. Ostroski, J. G. Meneguin, M. L. Gimenes, M.A.S.D. Barros, Study of Pb^{2+} adsorption in a packed bed column of bentonite using CFD, *Applied Clay Science*. 104 (2014) 48-58.

[44] W. Li, Adsorption characteristics of dyes in columns of activated carbon prepared from paper mill sewage sludge, *Chemical Engineering Journal.* 178 (2011) 197-203.

[45] T. Mitra, B. Singha, N. Bar, S. K. Das. Removal of Pb (II) ions from aqueous solution using water hyacinth root by fixed-bed column and ANN modeling, *Journal of Hazardous Materials.* 273 (2014) 94–103.

[46] C. P. Dwivedi, J. N. Sahu, C. R. Mohanty, B. R. Mohan, B. C. Meikap, Column performance of granular activated carbon packed bed for Pb (II) removal, *Journal of Hazardous Materials.*156 (2008) 596–603.

[47] R. Han, W. Zou, H. Li, Y. Li, J. Shi, 2006, Copper(II) and lead(II) removal from aqueous solution in fixed-bed columns by manganese oxide coated zeolite, *Journal of Hazardous Materials*. 137 (2006) 934–942.

[48] M.A. Mahmoud. Kinetics studies of uranium sorption by powdered corn cob in batch and fixed bed system, *Journal of Advanced Research*. 7 (2016) 79-87

[49] K. Mohanty, J. T. Naidu, B. C. Meikap, M. N. Biswas, Removal of crystal violet from wastewater by activated carbons prepared from rice husk, *Industrial and Engineering Chemistry Research*. 45(2006) 5165–5167.

[50] W. Wang, Z. Ding, M. Caic, H. Jianc, Z. Zengc, F. Lia, P. Liu. Synthesis and high-efficiency methylene blue adsorption of magnetic PAA/MnFe2O4 nanocomposites, *Applied Surface Science.* 346(2015)348–353.

[51] B. K. Nandi, A. Goswami, A. K. Das, B. Mondal, M. K. Purkait. Kinetic and grafted random copolymers of N-isopropylacrylamide and acrylic acid synthesized by RAFT polymerization: effect of different acrylic acid contents on LCST behavior, *RSC Advances.* 4(2008) 31428–31442.

[52] M. H. Dehghani, A. Dehghan, H. Alidadi, M. Dolatabadi, A. Mehrabpour, 2017, Removal of methylene blue dye from aqueous solutions by a new chitosan/zeolite composite from shrimp waste: kinetic and equilibrium study, *Korean Journal of Chemical Engineering*. 234(2017)1699–1707.

[53] G. Korneva, H. Ye, Y. Gogotsi, D. Halverson, G. Friedman, J. C. Bradley, K. G. Kornev, Carbon nanotubes loaded with magnetic particles. *Nano Letters*. 5(2008) 879–884.

HOW TO CITE THIS ARTICLE

Z. Hosseini Dastgerdi, S.S. Meshkat, H. Jalili, Investigation of an Adsorptive Indigo Carmine Dye Removal via Packed Bed Column: Experiments and Computational Fluid Dynamics Simulation, AUT J. Mech Eng., 4(3) (2020) 315-330.

DOI: 10.22060/ajme.2019.16920.5841